# The Dynamic Connection of the South Indian Ocean Countercurrent and the Leeuwin Current

Erwin Lambert, Dewi Le Bars, Will P. M. de Ruijter
Insitute of Marine and Atmospheric Sciences Utrecht, Utrecht University, the Netherlands

**Abstract**

The Leeuwin Current (LC) is an anomalous eastern boundary current flowing poleward along the western coast of Australia. Its forcing and dynamics are poorly understood. The LC is usually described by use of a regional coastal model, forced by a prescribed meridional gradient in density or sea surface topography offshore from the coastal region. The current study aims to place these dynamics in a perspective of surface forcing and inter-basin connections.

A hierarchy of two numerical models, an ocean general circulation model and a conceptual two-layer model, is used to study the shallow circulation of the South Indian and Pacific Oceans. A connection between the recently discovered Subtropical Indian Ocean Countercurrent (SICC) near Madagascar, and the meridional density gradient off the Australian coast is found. The SICC is part of a baroclinic system, formed by frontogenesis of meridionally tilted isopycnals. Along the zonal front, outcrop of isopycnals could be identified. The connection of this outcrop to the Australian coast was distinguished into two regimes. In the viscous regime, no coastal trapping is found and the SICC flows towards the southern coast of Australia. In the inertial regime, where eddies play a role, the outcrop was trapped along the western coast of Australia, connecting the SICC to the Leeuwin Current.

The return pathway of the Indonesian Throughflow (ITF) through the Indian Ocean was found to be partly trapped within the upper layers north of the outcrop line. It is redirected along this outcrop line, joining the eastward flow of the SICC. Shutdown of the ITF led to a strong decrease in Leeuwin Current transport and most of the SICC was found to connect to the internal gyre circulation in the Indian Ocean.

These results describe a mechanism for sustaining a poleward eastern boundary along an island, based on surface forcing. Furthermore, an explanation is given for the sensitivity of the LC to the ITF. Finally, it is reasoned that a strong LC can only exist due to the fact that there is a circulation around the island of Australia, and a similar current is therefore missing in other ocean basins.

## 1 Introduction

The South Indian Ocean (SIO) is anomalous from the world's other major ocean basins, because of three shallow currents. The first is the unique poleward flowing eastern boundary current (EBC), the Leeuwin Current (LC). Secondly, North of the Australian island, a relatively warm, fresh input from the Pacific is identified as the Indonesian Throughflow (ITF), with an estimated volume transport of 15 Sv (1 Sv = $10^6 m^3/s$) (Gordon et al., 2010). Third, in the west of the SIO, the Subtropical Indian Ocean Countercurrent (SICC, Palastanga et al. (2007); Siedler et al. (2006)) flows zonally off Madagascar, inducing an eastward transport which is found all the way to the Australian coast. This eastward transport is reflected in an equator-to-pole sea level drop of approximately 40cm along Australia (see Figure 1).

Recent studies have been complementary in focusing on the western and eastern SIO respectively, yet a coherent picture is missing. In the western SIO, observations have suggested the Agulhas Region as the origin of the SICC (Nauw et al., 2008). In the east, observations (Smith et al., 1991; Woo et al., 2006; Woo and Pattiaratchi, 2008; Weller et al., 2011) and Lagrangian models (Song et al., 2004; Domingues et al., 2007; Valsala and Ikeda, 2007; van Sebille et al., 2014) have found both tropical (including ITF) and subtropical waters to be a source for the LC. Basin-wide observations as shown in Figure 1 show that westward flow around 10°S (partly ITF) and eastward flow near 22° (SICC) cross the entire basin of the Indian Ocean, suggesting large-scale connections between the east and west. Overall, however, dynamical understanding of the connection between these three shallow currents, the LC, the SICC and the ITF, is insufficient and has not explained the basin-wide connectivity.

The LC has acquired much attention due to its fundamental interest and relevance for local climate and ecology (Waite et al., 2007). Linear theory can not explain a poleward boundary current along the eastern boundary. Early studies have pointed towards observed meridional gradients in density and steric height as a forcing agent for the LC and the influence of the ITF in reinforcing these gradients (Godfrey and Ridgway, 1985; Weaver and Middleton, 1989). Theories on the coastal trapping of the LC have focused on vertical diffusion of Rossby waves (McCreary et al., 1986) and interaction with the continental shelf (Csanady, 1978, 1985) and a current program is evaluating the various proposed mechanisms (Furue et al., 2013; Benthuysen et al., 2013).

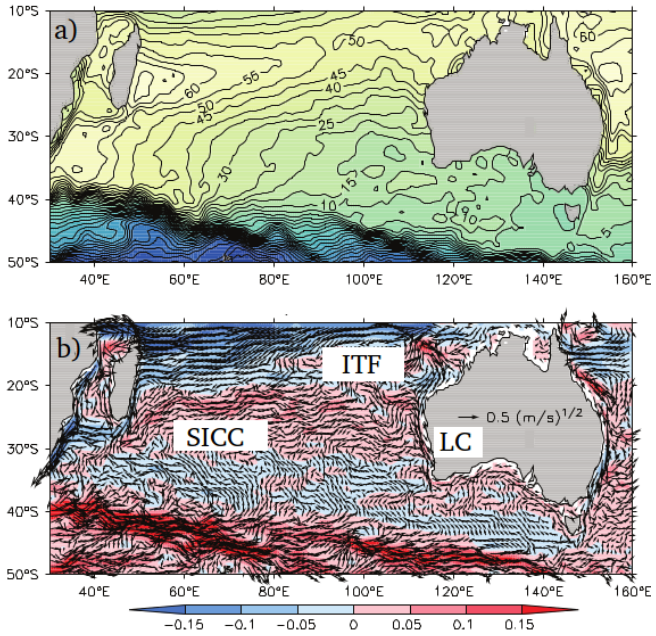


**Figure 1:** Observations of the South Indian Ocean. a) Mean sea surface topography (cm) from altimetry. b) Horizontal currents at 46m depth from SODA-POP reanalysis in $(\mathrm{m/s})^{1/2}$. Positive values indicate an eastward component. Adapted from Schott et al. (2009).

The SICC shows many similarities to other Subtropical Countercurrents (STCCs) which have been identified in the North Pacific (Uda and Hasunuma, 1969), South Pacific (Merle et al., 1969), North Atlantic (Reid, 1978) and South Atlantic (Tsuchiya, 1985). These zonal currents have the clearest signature near 25°N/S in the western part of the basin. Effort to study the dynamics of these countercurrents and the mechanism of frontogenesis has spanned decades. Suggested mechanisms are Ekman convergence (Takeuchi, 1984), isothermal $\beta$-convergence (Cushman-Roisin, 1984), advection of mixed-layer depth (De Ruijter, 1983), convergence of Rossby waves (Dewar, 1987, 1991, 1992) and mode water formation (Kubokawa, 1997, 1999; Kubokawa and Inui, 1999). A clear overview of this process of development was given by Kobashi and Kubokawa (2011). Although no agreement is found so far on a single mechanism, and all may play a part in the actual frontogenesis forming these STCCs including the SICC, all studies agree that it is due to a combination of buoyancy forcing and wind stress. The meridional gradient in buoyancy forcing slopes the isopycnals, and interaction with the wind-driven gyre produces convergence, leading to a narrow baroclinic jet. Because these fronts are expressed in a sharp gradient of isopycnal depth, these isopycnals can outcrop along the fronts of the STCCs.

The effect of the ITF on the circulation system in the SIO was first studied with a General Circulation Model (GCM) by Hirst and Godfrey (1993), performing simulations in which the Indonesian Passages were closed in one run and open in another. In the run allowing the ITF, a shallow southeastward jet was found near the latitude where the SICC is observed, down to the southwestern point of Australia. In the closed run, blocking the ITF, this shallow circulation was weakened, indicating that this system is sensitive to ITF input. They suggested that the Leeuwin Current System (LCS) is part of this shallow circulation. However, due to the coarse resolution, no boundary currents could be resolved. Their results were supported by a model-intercomparison study by McCreary et al. (2007) and similar features were found in three models of different complexity. A first study with open and closed Indonesian Passages at eddy-resolving resolution was performed by Le Bars et al. (2013). Since analysis of these model results was restricted to barotropic circulation, no conclusions were drawn on the SICC and LC systems. Among other things, this study highlights the necessity of high-resolution numerical modeling to resolve realistic regimes in boundary regions.

The current study aims to unravel the large-scale connectivity and governing dynamics of the general circulation in the shallow SIO, with a focus on the LC and the SICC. Questions that will be addressed are: What is the dynamic connection between the SICC and the LC? How can the general features of the shallow circulation in the SIO be understood from surface forcing? What is the role of the ITF in this system? Why are poleward EBCs like the LC not found in other basins?

To answer these questions, two models of different complexity are used. Firstly, an ocean GCM is run at high and coarse resolution to validate against the results of Hirst and Godfrey (1993), and to reveal the inertial effects of the sensitivity of the LCS to the ITF. Secondly, a conceptual regional two-layer model is used to simulate the general shallow circulation features of the SIO from surface forcing and to reveal the sensitivity of these features to removal of the circulation around Australia.

In Section 2, properties and configuration of both models are presented. Results of the GCM study are shown in Section 3 and the results of the conceptual model in Section 4. With both models, sensitivity of the circulation to the ITF is presented in Section 5, which is followed by a summary and discussion in Section 6.

## 2 Model configurations

Two models were used in this study to reveal the dynamics of the shallow circulation in the SIO, one ocean GCM and one conceptual two-layer model. The basic properties as well as the configuration of both models are explained in the following subsections.

### 2.1 General Circulation Model: Parallel Ocean Program

The Parallel Ocean Program (POP, Dukowicz and Smith (1994)) is an ocean-only general circulation model solving the primitive equations on a horizontal grid of av-

erage resolution of 0.1° and 42 vertical layers. The atmospheric state and precipitation were taken from the CORE dataset (Large and Yeager, 2004), wind stress is computed offline using Hurrell Sea Surface Temperature climatology (Hurrell et al., 2008) and evaporation and sensible heat flux were calculated online. Bulk formulae are applied rather than restoring.

Data were used from the simulations performed by Le Bars et al. (2013). After a spin-up of 75 years as described by Maltrud et al. (2009), two simulations were performed, one with realistic bathymetry, the other with closed Indonesian Passages in a similar fashion as Hirst and Godfrey (1993). Both were run for another 105 model years of which the last 50 years of simulation were averaged to approximate the steady-state solution. Simulations were repeated on a horizontal grid with average resolution of 1.0° allowing for validation against previous modeling studies.

## 2.2 Conceptual model: Hallberg Isopycnal Model

The Hallberg Isopycnal Model (HIM, (Hallberg, 1997, 1999)) is a regional ocean-only model solving the hydrostatic primitive equations in spherical coordinates on an Arakawa C-grid. It is configured to an idealized representation of the Indian and Pacific Ocean, separated by an elongated island, representing Australia, see Figure 2. A minimum of idealized forcing terms is applied to simulate a mid-ocean eastward jet in the western basin, and a westward jet along the northern boundary of Australia with a predictable return pathway. These jets will be interpreted as the SICC and the ITF respectively.

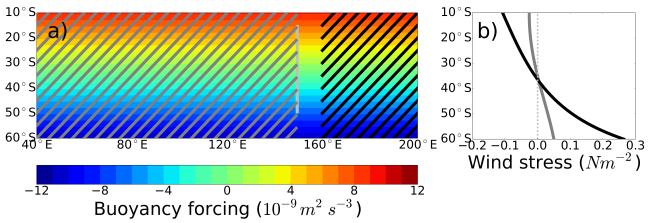


**Figure 2:** Configuration of the conceptual two-layer model. a) Model domain, applied buoyancy forcing (shading) and two areas where wind stress is applied (hatches). The light grey area at 150° indicates the elongated island. b) Wind stress simulating a gyre (grey) and ITF (black) applied to respective areas as indicated in the left panel.

A small eastern basin is taken, compared to the actual Pacific Ocean it represents, to save computing time. Over the entire domain, the bottom is flat with a depth of 1500m below the free surface, which is the approximate depth of the wind-driven circulation. The island is elongated to reduce effects of eddy shedding due to lateral friction at the northern and southern boundaries. Because of the baroclinic structure of the Indian Ocean circulation, where both SICC and LC have observed opposite flow in deeper layers, a minimum of 2 layers is needed to qualitatively describe these features. As initial state, the interface depth between these layers was taken constant at 100m, a typical depth of both the SICC and the LC. Stratification of the model is based on the 20° isotherm determined using Argo float data from the ARIVO project (Gaillard and Charraudeau, 2008) over the corresponding domain and depths. The constant density of the upper layer was thus defined by the average density above the 20° isotherm. Density of the lower layer was defined as the average density between the isotherm and 1500m depth. The respective densities are $\rho_1$=1028.9 and $\rho_2$=1031.6$kgm^{-3}$. After spin-up, as described below, the mean interface depth is 200m, giving mean depths of the layers $H_1 = 200m$ and $H_2 = 1300m$ This stratification gives an internal Rossby radius of deformation,

$$R_{int} = \frac{1}{f}\sqrt{\frac{g' H_1 H_2}{H_1 + H_2}}, \tag{1}$$

of 22km, where $g' = g\frac{(\rho_2 - \rho_1)}{\rho_0}$ is the reduced gravity and $f = 10^{-4}s^{-1}$ is the Coriolis parameter at midlatitudes. This value puts a requirement on the horizontal resolution. A horizontal resolution of 0.2° was taken, giving an approximate grid size of 20km, thus resolving eddies. To investigate both inertial and viscous response in the boundary layer regions, two values for horizontal Laplacian viscosity are taken. The inertial boundary layer width is approximated as

$$\delta_I = \sqrt{\frac{U}{\beta_0}}, \tag{2}$$

where $U = O(10^{-2})ms^{-1}$ is a typical velocity scale in the interior, giving $\delta_I = 22km$. The width of the Munk layer is dependent on the horizontal Laplacian viscosity $A_H$, through

$$\delta_M = \sqrt[3]{\frac{A_H}{\beta_0}}. \tag{3}$$

This value is 17km and 79km for $A_H = 100m^2s^{-1}$ and $10^4m^2s^{-1}$ respectively. Hence, for the low viscosity, the inertial boundary layer is dominant and this simulation can be defined as the inertial regime. For the high viscosity, the Munk layer is dominant and this simulation is defined as the viscous regime. This viscous regime may be compared to coarse simulations from previous studies (Hirst and Godfrey, 1993; McCreary et al., 2007). Along the lateral boundaries, no-slip conditions were applied.

To simulate the effect of heating and fresh water forcing at the surface, a total buoyancy forcing is applied, following the ideas of Haney (1971). In analogy to the surface boundary condition for heating,

$$\frac{Q}{\rho_0 C_p} = K_v \frac{\partial T}{\partial z}, \tag{4a}$$

a boundary condition for buoyancy forcing can be written as

$$\frac{B\rho_0}{g} = -K_v \frac{\partial \rho}{\partial z}. \tag{4b}$$

Here, a linear equation of state is assumed, and thus

$$\frac{\partial \rho}{\partial T} = -\rho_0 \alpha, \tag{4c}$$

and buoyancy can be related to Q via

$$B = \frac{g\alpha}{\rho_0 C_p} Q \tag{4d}$$

Here, $Q$ is the net surface heat flux in $Wm^{-2}$; $\rho_0 = 1035 kgm^{-3}$ is the reference density; $C_p = 4181 JK^{-1}kg^{-1}$ is the heat capacity of water; $K_v$ is the vertical diffusivity; $g = 9.81 ms^{-2}$ is the gravitational acceleration; $\alpha = 1.7 * 10^{-4} K^{-1}$ is the coefficient of thermal expansion; and $B$ is the surface buoyancy forcing in $m^2 s^{-3}$. The maximum value of $12 * 10^{-9} m^2 s^{-3}$ is equivalent to a surface heat flux of $30 Wm^{-2}$, a moderate value compared to estimates by Haney (1971). The applied buoyancy forcing has a constant meridional gradient and is independent on longitude as can be seen in Figure 2. The total buoyancy forcing is conserved over the ocean surface.

The applied wind stress is divided into two domains, indicated by the grey and black boxes in Figure 2. The profiles are based on Sverdrup theory, stating, when assumed that all configuration is independent on longitude and meridional wind stress is zero,

$$\beta v = \frac{1}{\rho D} \frac{\partial \tau^x}{\partial y}. \tag{5}$$

Here, $\beta = 2 * 10^{-11} m^{-1} s^{-1}$ is the meridional derivative of the Coriolis parameter; $D = 1500m$ is the total depth and $\tau^x$ is the zonal wind stress in $Nm^{-2}$. Historically, gyres are simulated by applying a sinusoid wind stress. This leads to a maximum meridional velocity at the maximum wind-curl line and zero meridional velocity at the zero wind-curl line. To find the total meridional transport through a line of constant latitude, integration over the longitudinal extent is taken. Hereby, the sinusoid wind-stress applied in the western basin (grey box) is corrected for the earth's curvature. This leads to stronger westerly winds in the south, compared to easterlies in the north, resembling observations. In a similar fashion, the applied wind stress in the eastern basin (black box), simulating an ITF-like jet, is taken to be a constant wind-stress curl, corrected to give a constant northward transport of 15 Sv according to Sverdrup theory. Depth-integrated return flow of this transport is required to follow the northern, western and southern boundaries, thus producing a circulation around the island. To reduce effects of lateral friction at the boundaries of the island, this wind stress is applied at a distance of 10° off the island's eastern boundary and sufficient gaps are left at the north and south. Because of the relatively large area of wind forcing in the western basin compared to the eastern basin, lower values for wind stress were taken in the west to reach comparable transport values.

Since outcrop is allowed and is expected to follow from the frontogenesis mechanism, part of the basin will effectively become a one-layer column which cannot dissipate the applied buoyancy forcing downward. This breaks down the conservation of energy and as a net effect, the mean interface will sink due to the positive buoyancy excess. A two-layer system with outcrop can therefore not reach a steady state. The timescale of interface sinking due to this process is much longer than the timescale of initial adjustment. After 50 model years, total energy in the system was found to be approximately constant. From this moment onwards, a slight increase was found, reflecting the slow adjustment towards a state of no outcrop. Since we wish to study the effect of outcrop, as is observed in the real ocean and in GCM simulations, the steady-state approximation is made around the separation of these timescales of adjustment. To this purpose, values are averaged over the period between model years 45 and 55.

Linear theory allows qualitative prediction of the resulting circulation, and it is instructive to do so before analysing the results. The depth-integrated circulation is expected to be a sum of a Sverdrup gyre in the western basin and a jet-like circulation along the northern, western and southern boundaries, connecting to the broad constant northward flow in the far eastern basin. The linear meridional gradient in buoyancy forcing is expected to produce a baroclinic structure of broad eastward flow over the whole domain in the upper layer, and westward return flow in the lower layer, according to thermal wind balance:

$$\frac{\partial u}{\partial z} = \frac{g}{\rho_0 f} \frac{\partial \rho}{\partial y} \tag{6}$$

Interaction between the gyre and buoyancy gradient has been shown to produce frontogenesis in the mid-ocean (Takeuchi, 1984; Cushman-Roisin, 1984), and could lead to outcrop in the south. Due to this frontogenesis mechanism, the eastward flow in the upper layer is expected to become more narrow, resembling the observed STCCs like the SICC.

# 3 GCM results

Steady state solutions of the GCM simulations with the POP model in two resolutions are shown in Figure 3. Panel a) shows a shallow current system in the viscous regime, which is similar to Hirst and Godfrey (1993). The mid-latitudes are dominated by an eastward flow, bending southward to the southwestern point of Australia. Hirst and Godfrey (1993) suggested that this circulation was connected to the LCS, yet the coarse resolution could not resolve this boundary current system. To realistically resolve the boundary regions, and to allow for inertial effects, the same model is configured to eddy-resolving resolution (0.1x0.1°). These solutions, shown in Figure 3b), show a clear poleward flowing Leeuwin Current.

Both solutions show zonal departure of the SICC from Madagascar, with a northward branch bifurcat-

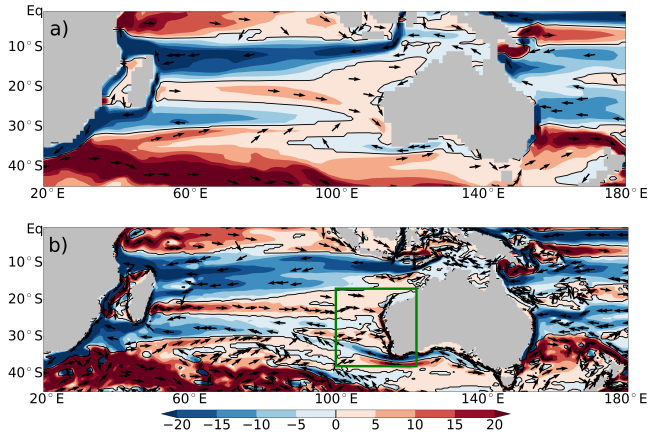


**Figure 3:** Horizontal velocities integrated over the top 200m ($m^2s^{-1}$, or Sv/1000km). Positive values indicate an eastward component, the thin black line indicates the border between eastward and westward components. Unit vectors are added at local maxima to show the direction of the flow. a) The steady-state solution of the GCM simulations in coarse resolution (1.0x1.0°). b) The same in the high resolution case (0.1x0.1°). The green box indicates the area shown in Figure 4

ing near 90°E. This is possibly due to interaction with the topography of the 90°E ridge. Another possible explanation for the bifurcation is the nearby subduction area, affecting subsurface potential vorticity and thereby sloping isopycnals. This last mechanism was suggested to explain the bifurcation of the North Pacific STCC by Kobashi et al. (2006). The northern branch of the SICC reaches the North-West shelf, where it feeds into the coastal jet. The southern branch reaches Australia just south of the North West Cape. Transects were taken at regular intervals of 2° along the Australian coast to quantify the LC transport (see Figure 4). Upstream of the North West Cape (22°S, transect F), low transport values are found. A sharp increase from approximately 0.5 to 2.5 Sv is found just south of the North West Cape, which is the latitude of the extention of the SICC.

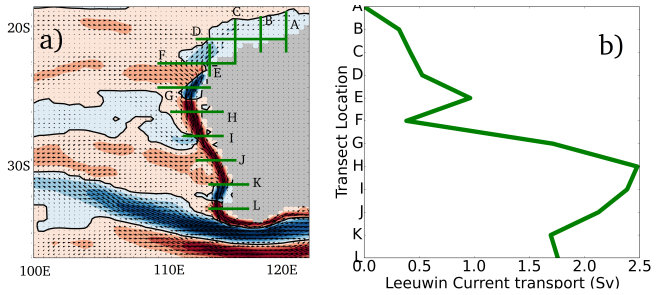


**Figure 4:** a) Inlet from Figure 3 with indicated transects along the western coast. Transects are taken at intervals of 2° along the coast. Labels A-L are ordered from up- to downstream where A,B,C and E are meridional sections, the others zonal. b) Calculated transport values of the LC through the transects. Transect F is at the latitude of the North West Cape of 22°

These results provide evidence that also in the eddy-resolving regime, the shallow eastward flow identified as the SICC, connects to the southwest of Australia, yet its southward flow is trapped along the coast, thus forming the Leeuwin Current. To explain this mechanism, the conceptual two-layer model is used with idealized surface forcing terms.

# 4 Conceptual model results

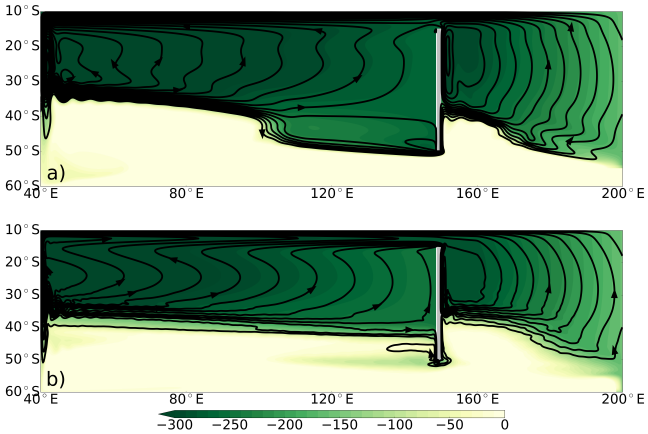


**Figure 5:** Streamlines (contours, interval 1 Sv) of a) viscous and b) inertial circulation in the upper layer as forced by the configuration shown in Figure 2. Shading indicates the depth of the interface relative to the free surface in meters.

From the upper layer velocities simulated as described in Subsection 2.2, streamfunctions are determined. This is done by integrating velocity gradients along zonal and meridional paths from each corner. This leads to 8 possible integration paths, and all were averaged to give a best estimate of the streamfunction. Averaging is needed since the upper layer volume is not conserved, but slowly increases due to the net buoyancy input as described in Subsection 2.2. These streamfunctions are shown in Figure 5 for both viscous (panel a) and inertial (panel b) simulations. In the viscous circulation, similar features can be distinguised as were found by Hirst and Godfrey (1993) and in the coarse resolution GCM results as described in the previous section. Off the western boundary, a narrow zonal mid-ocean current departs. It bends southeastward to converge toward the southwestern point of the island. The apparent discontinuity near 100°E is a westward propagating Rossby wave and no steady feature. Over the whole period, no coastal trapping was found, and this Rossby wave will dissipate in the western boundary region, smoothening the outcrop line. The mid-ocean jet follows from thermal wind balance in a two-layer system:

$$u_1 - u_2 = \frac{g'}{f}\frac{\partial h}{\partial y}, \tag{7}$$

where $u_1$ and $u_2$ are the zonal velocities (in $ms^{-1}$) in the upper and lower layer respectively and h is the interface depth in meters. Here, h is sloped due to surface buoyancy forcing. $\frac{\partial h}{\partial y}$ is increased due to frontogenesis

as described below. This leads to large values of velocity shear along this outcrop line.

To resolve the inertial regime, the simulation was repeated with a horizontal viscosity of $100m^2s^{-1}$ (panel b). It can be seen that the mid-ocean jet nearly retains its latitude, and flows zonally toward the western coast of the island. A coastally trapped poleward current is formed to allow circulation toward the eastern basin. The coastal trapping is likely due to the same mechanism of vertical diffusion of Rossby waves as described by McCreary et al. (1986), since the chosen diapycnal diffusivity of $1cm^2s^{-1}$ was found to allow this diffusion. To simulate a Leeuwin Current, McCreary et al. (1986) prescribed an offshore meridional gradient in surface density of approximately $3kgm^{-3}$ over a meridional extent of 20°, or 2000km. This value was based on observations and is similar to our high resolution GCM simulations. Combining equations 6 and 7, an estimate can be made of the gradient in isopycnal depth to produce an equivalent onshore forcing to the surface density gradient. The velocity shear $\frac{\partial u}{\partial z}$ from equation 6 is approximately $1.5{*}10^{-4}s^{-1}$. Assuming $\frac{\partial u}{\partial z} = \frac{u_1 - u_2}{(H_1+H_2)/2}$ is the representation of velocity shear in the two-layer model, this can be combined with equation 7 to give a value for $\frac{\partial h}{\partial y}$, which is $3 * 10^{-4}$. The typical meridional extent of the isopycnal tilt, as can be seen in Figure 5 is 10°, or 1000km. This combines to an equatorward drop in isopycnal depth of approximately 300m, which is indeed found.

This order-of-magnitude estimation shows that using surface forcing in the two-layer model gave an equivalent onshore forcing to drive the Leeuwin Current, as was prescribed by McCreary et al. (1986) and as was found in the GCM simulations. Together with the parametrization of diapycnal diffusivity, this suggests that the mechanism for coastal trapping in the two-layer model is also due to Rossby wave diffusivity.

The observed frontogenesis mechanism is most likely dominated by Ekman convergence:

$$V = \frac{-\tau^x}{\rho_0 f} \tag{8}$$

This mechanism converges the upper layer to the zero wind stress line at 35°S. Due to negative buoyancy forcing in the south, the interface is lifted into this Ekman layer, and advected northward towards the convergence line. In this process, all upper layer water is transported across the convergence line, and outcrop of the interface in the south takes place. Observed STCCs are approximately 10° closer to the equator than the Ekman convergence line, this is most likely due to feedback with the atmosphere and subduction which are not reproduced in the model. Still, the outcropping interface resembles the observed thermocline shape in the Indian Ocean. Furthermore, the outcrop is trapped along the western coast of the island, therefore sustaining a baroclinic system resembling the LCS.

# 5 Sensitivity to ITF

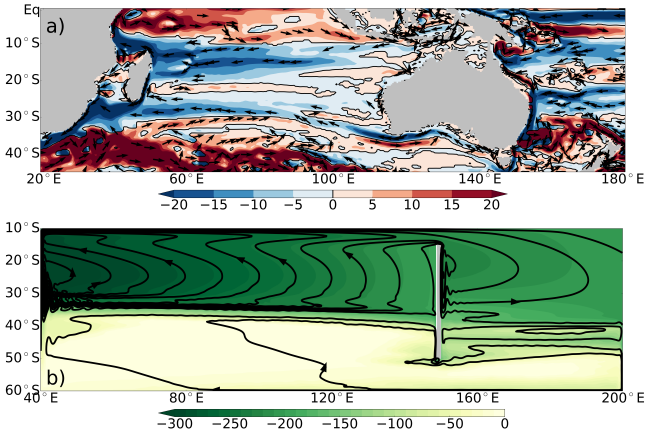


**Figure 6:** Upper panel: integrated horizontal velocities ($m^2/s$) over the top 200m from POP simulations with closed Indonesian Passages. Lower panel: streamfunction of the upper layer (contours in 1 Sv) simulated with HIM as described in Section 2.2 without the wind forcing in the eastern basin (black area).

Sensitivity of the Indian Ocean circulation to the ITF was studied by Hirst and Godfrey (1993) with a coarse resolution GCM. They found that closure of the Indonesian Passages decreased the shallow eastward flow and the LCS. The resulting circulation in our eddy-resolving GCM simulations with closed Indonesian Passages is shown in Figure 6a. Comparison with Figure 3b shows that when more accurately resolving the inertial regimes of the SICC and the LC, both currents indeed decrease due to blocking of the ITF as was found in the viscous simulations of Hirst and Godfrey (1993).

To understand this sensitivity, the method of ITF simulation in the conceptual allows for removal of this inflow. Setting the wind stress east of the island (black hatches in Figure 2b) to zero will produce zero transport through the gap north of the island. This has a benefit over closure of the opening north of the island and leaving the wind stress as it is: closing this passage, as was done in the GCM simulations, will induce a western boundary current in the eastern basin and could induce leakage south of the island, similar to Tasman Leakage, which was found to increase due to blocking of the ITF in the POP model (Le Bars et al., 2013). The resulting circulation without wind stress over the eastern basin is shown in the Figure 6b. A decreased transport along the mid-ocean front is found, and the connection of the poleward boundary currents in the east and west is broken.

We find here that, in absence of the inflow from the eastern basin, the mid-ocean jet connects to the interior gyre. To connect this jet, resembling the SICC to the poleward EBC, resembling the Leeuwin Current, circulation around the island is necessary. When inflow from the eastern to the western basin is allowed along

the north of the island, part of this island circulation appears to be trapped in the upper layer by limited diapycnal transport. It follows the southern boundary of this upper layer, which is the outcrop line.

Opposite to current views, the mechanism described here does not connect the ITF to the LC directly. Rather, these two currents are connected through the SICC. With this mechanism, two requirements for the island circulation are met. Firstly, the transport forced in the upper layer east of the island returns along the southern boundary of this upper layer, which is the outcrop line and the coastal areas of the island. Secondly, the depth-integrated transport agrees with linear theory and follows the western boundary region all the way to the latitude of zero wind curl which is the southern boundary (not shown). To meet these requirements, transport in the lower layer produces an opposite flow against the shallow SICC-LC system which is in agreement with observations where a Leeuwin Undercurrent is found, as well as westward flow in the subthermocline Indian Ocean.

# 6 Conclusions and discussion

Simulations with two models of different complexity have provided evidence for a new dynamic connection between the ITF and the LC, namely through the western boundary of the Indian Ocean and the SICC. GCM simulations show that the majority of LC transport is fed just south of the North West Cape at 22°, where the extention of the SICC is found. Comparison with coarse resolution simulations and results from Hirst and Godfrey (1993) showed that this connection is found in both viscous and inertial regimes. In the latter, an actual poleward eastern boundary current is found.

In a two-layer model, a shallow zonal mid-ocean jet was simulated using a combination of wind stress and buoyancy forcing. Frontogenesis through Ekman convergence produced outcrop and a narrow baroclinic system. These results are in agreement with previous attempts to produce STCCs in a conceptual model (Takeuchi, 1984; Cushman-Roisin, 1984).

It is found that an induced circulation around an island in the east of the basin was partly trapped within the upper layer. Return flow joined the mid-ocean jet rather than flowing towards the southern boundary of the basin. By varying the horizontal viscosity, a distinction could be made between a viscous and an inertial regime. In the inertial regime, the return flow was trapped along with the outcrop line, inducing an EBC. This mechanism of coastal trapping is in agreement with the theory proposed by McCreary et al. (1986).

Although poleward EBCs were found in the two-layer model in absence of the island circulation (see Figure 6b), these are formed due to a limitation of the model. Outcrop is not sustained along the southern boundary, hence inducing a baroclinic circulation. Realistically, no low density water is found at these latitudes, and thus no such circulation will be found in GCM simulations, or in the real ocean when the ITF is absent. For a realistic LC to develop, inflow from the Pacific is necessary.

To stay away from effects of choking in the two-layer model, a large gap north of the island is taken. The actual Indonesian Passages are much more narrow. Therefore, no return flow is found along the north of the island, in contrast with the two-layer simulations. Also, the Passages are shallow, forcing more ITF into the layers of low density. Together, the amount of return flow from the ITF along this pathway of the SICC and LC is underestimated in these simulations. Yet, the actual inflow of the LC into the Pacific is limited due to subduction south of Australia. This subduction connects the upper and lower layers and produces a zonal overturning circulation within the Indian Ocean, rather than circulation around the island. Finally, the observed direct input of the ITF into the LC, giving the LC a relatively tropical structure, can be understood from Ekman transport, forcing the ITF southward. This direct connection, however, cannot explain the forcing of the LC and for this, the SICC is needed.

In this study, a new mechanism is proposed for the forcing and large-scale connections of the Leeuwin Current. It requires the circulation around Australia through the ITF, and the outcrop associated with the SICC. This mechanism is qualitatively described in terms of an idealized two-layer configuration based on surface forcing terms. In conclusion, these results add new insights in the understanding of the LC dynamics and may provide a large-scale background structure for regional models describing the Leeuwin Current.

# Acknowledgements

*I would like to thank firstly Fi and Wytze for all the discussions and feedback on this thesis and for the overall support throughout these last 9 months. Furthermore, thanks to Leon, Sharon, Sjoerd, Lotte, Felix, Roeland, Timo and all the other students for making this stressful period of graduation bearable. Without the work of Michael Kliphuis, no simulations would have been performed with either model. I am very grateful for the amount of time and effort Dewi Le Bars has put into this project, his enthousiasm for solving any problem I could think of kept me going. And final thanks are directed to Will de Ruijter for giving me all this freedom and inexhaustible support throughout the thesis.*

# References


J. Benthuysen, R. Furue, J. P. McCreary, N. L. Bindoff, and H. E. Phillips. Dynamics of the Leeuwin Current: Part 2. Impacts of mixing, friction, and advection on a buoyancy-driven eastern boundary current over a shelf. *Dynamics of Atmospheres and Oceans*, Nov. 2013. ISSN 03770265. doi: 10.1016/j.dynatmoce.2013.10.004.

G. T. Csanady. The Arrested Topgraphic Wave. *Journal of Physical Oceanography*, 8:47–62, 1978.

G. T. Csanady. "Pycnobathic" Currents over the Upper Continental Slope. *Journal of Physical Oceanography*, 15:306–315, 1985.

B. Cushman-Roisin. On the Maintenance of the Subtropical Front and its Associated Countercurrent. *Journal of Physical Oceanography*, 14: 1179–1190, 1984.

W. P. M. De Ruijter. Frontogenesis in an Advective Mixed-Layer Model. *Journal of Physical Oceanography*, 13:487–495, 1983.

W. K. Dewar. Planetary Shock Waves. *Journal of Physical Oceanography*, 17:470–482, 1987.

W. K. Dewar. Arrested fronts. *Journal of Marine Research*, 49:21–52, 1991.

W. K. Dewar. Spontaneous Shocks. *Journal of Physical Oceanography*, 22:505–522, 1992.

C. M. Domingues, M. E. Maltrud, S. E. Wijffels, J. a. Church, and M. Tomczak. Simulated Lagrangian pathways between the Leeuwin Current System and the upper-ocean circulation of the southeast Indian Ocean. *Deep Sea Research Part II: Topical Studies in Oceanography*, 54(8-10):797–817, Apr. 2007. ISSN 09670645. doi: 10.1016/j.dsr2.2006.10.003.

J. K. Dukowicz and R. D. Smith. Implicit free-surface method for the Bryan-Cox-Semtner ocean model. *Journal of Geophysical Research*, 99(C4):7991, 1994. ISSN 0148-0227. doi: 10.1029/93JC03455.

R. Furue, J. P. McCreary, J. Benthuysen, H. E. Phillips, and N. L. Bindoff. Dynamics of the Leeuwin Current: Part 1. Coastal flows in an inviscid, variable-density, layer model. *Dynamics of Atmospheres and Oceans*, 63:24–59, Sept. 2013. ISSN 03770265. doi: 10.1016/j.dynatmoce.2013.03.003.

F. Gaillard and R. Charraudeau. New climatology and statistics over the global ocean. *MERSEA del*, 5(7), 2008.

J. S. Godfrey and K. R. Ridgway. The Large-Scale Environment of the Poleward-Flowing Leeuwin Current, Western Australia: Longshore Steric Height Gradients, Wind Stresses and Geostrophic Flow. *Journal of Physical Oceanography*, 15:481–495, 1985.

A. L. Gordon, J. Sprintall, H. M. van Aken, D. Susanto, S. E. Wijffels, R. Molcard, A. Ffield, W. Pranowo, and S. Wirasantosa. The Indonesian throughflow during 2004–2006 as observed by the INSTANT program. *Dynamics of Atmospheres and Oceans*, 50(2):115–128, Aug. 2010. ISSN 03770265. doi: 10.1016/j.dynatmoce.2009.12.002.

R. Hallberg. HIM: The Hallberg Isopycnal Coordinate Primitive Equation Model, 1997.

R. Hallberg. Time Integration of Diapycnal Diffusion and Richardson Number – Dependent Mixing in Isopycnal Coordinate Ocean Models. *Monthly Weather Review*, 128(1993):1402–1419, 1999.

R. L. Haney. Surface Thermal Boundary Conditions for Ocean Circulation Models. *Journal of Physical Oceanography*, 1(4):241–248, 1971.

A. C. Hirst and J. S. Godfrey. The Role of Indonesian Throughflow in a Global Ocean GCM. *Journal of Physical Oceanography*, 23, 1993.

J. W. Hurrell, J. J. Hack, D. Shea, J. M. Caron, and J. Rosinski. A New Sea Surface Temperature and Sea Ice Boundary Dataset for the Community Atmosphere Model. *Journal of Climate*, 21(19):5145–5153, Oct. 2008. ISSN 0894-8755. doi: 10.1175/2008JCLI2292.1.

F. Kobashi and A. Kubokawa. Review on North Pacific Subtropical Countercurrents and Subtropical Fronts: role of mode waters in ocean circulation and climate. *Journal of Oceanography*, 68(1):21–43, Nov. 2011. ISSN 0916-8370. doi: 10.1007/s10872-011-0083-7.

F. Kobashi, H. Mitsudera, and S.-P. Xie. Three subtropical fronts in the North Pacific: Observational evidence for mode water-induced subsurface frontogenesis. *Journal of Geophysical Research*, 111 (C09033):1–16, 2006. ISSN 0148-0227. doi: 10.1029/2006JC003479.

A. Kubokawa. A Two-Level Model of Subtropical Gyre and Subtropical Countercurrent. *Journal of Oceanography*, 53:231–244, 1997.

A. Kubokawa. Ventilated Thermocline Strongly Affected by a Deep Mixed Layer : A Theory for Subtropical Countercurrent. *Journal of Physical Oceanography*, 29:1314–1333, 1999.

A. Kubokawa and T. Inui. Subtropical Countercurrent in an Idealized Ocean GCM. *Journal of Physical Oceanography*, 29:1303–1313, 1999.

W. G. Large and S. G. Yeager. *Diurnal to decadal global forcing for ocean and sea-ice models: the data sets and flux climatologies*. National Center for Atmospheric Research, 2004.

D. Le Bars, H. A. Dijkstra, and W. P. M. De Ruijter. Impact of the Indonesian throughflow on Agulhas leakage. *Ocean Science Discussions*, 10(1):353–391, Feb. 2013. ISSN 1812-0822. doi: 10.5194/osd-10-353-2013.

M. Maltrud, F. Bryan, and S. Peacock. Boundary impulse response functions in a century-long eddying global ocean simulation. *Environmental Fluid Mechanics*, 10(1-2):275–295, Oct. 2009. ISSN 1567-7419. doi: 10.1007/s10652-009-9154-3.

J. P. McCreary, S. R. Shetye, and P. K. Kundu. Thermohaline forcing of eastern boundary currents: With application to the circulation off the west coast of Australia. *Journal of Marine Research*, 44(1):71–92, Feb. 1986. ISSN 00222402. doi: 10.1357/002224086788460184.

J. P. McCreary, T. Miyama, R. Furue, T. Jensen, H.-W. Kang, B. Bang, and T. Qu. Interactions between the Indonesian Throughflow and circulations in the Indian and Pacific Oceans. *Progress in Oceanography*, 75(1):70–114, Oct. 2007. ISSN 00796611. doi: 10.1016/j.pocean.2007.05.004.

J. Merle, H. Rotschi, and B. Voituriez. Zonal Circulation in the Tropical Western South Pacific at 170E. *Bulletin of the Japanese Society of Fisheries Oceanography*, pages 91–98, 1969.

J. J. Nauw, H. M. van Aken, A. Webb, J. R. E. Lutjeharms, and W. P. M. De Ruijter. Observations of the southern East Madagascar Current and undercurrent and countercurrent system. *Journal of Geophysical Research*, 113(C8):C08006, Aug. 2008. ISSN 0148-0227. doi: 10.1029/2007JC004639.

V. Palastanga, P. J. van Leeuwen, M. W. Schouten, and W. P. M. De Ruijter. Flow structure and variability in the subtropical Indian Ocean: Instability of the South Indian Ocean Countercurrent. *Journal of Geophysical Research*, 112(C1):C01001, Jan. 2007. ISSN 0148-0227. doi: 10.1029/2005JC003395.

J. L. Reid. On the middepth circulation and salinity field in the North Atlantic Ocean. *Journal of Geophysical Research*, 83(C10):5063, 1978. ISSN 0148-0227. doi: 10.1029/JC083iC10p05063.

F. A. Schott, S.-P. Xie, and J. P. McCreary. INDIAN OCEAN CIRCULATION AND CLIMATE VARIABILITY. *Reviews of Geophysics*, (47):1–46, 2009. doi: 10.1029/2007RG000245.1.INTRODUCTION.

G. Siedler, M. Rouault, and J. R. E. Lutjeharms. Structure and origin of the subtropical South Indian Ocean Countercurrent. *Geophysical Research Letters*, 33(24):L24609, Dec. 2006. ISSN 0094-8276. doi: 10.1029/2006GL027399.

R. L. Smith, A. Huyer, J. S. Godfrey, and J. A. Church. The Leeuwin Current off Western Australia, 1986-1987. *Journal of Physical Oceanography*, 21:323–345, 1991.

Q. Song, A. L. Gordon, and M. Visbeck. Spreading of the Indonesian Throughflow in the Indian Ocean *. *Journal of Physical Oceanography*, 34:772–792, 2004.

K. Takeuchi. Numerical Study of the Subtropical Front and the Subtropical Countercurrent. *Journal of the Oceanographical Society of Japan*, 40:371–381, 1984.

M. Tsuchiya. Evidence of a double-cell subtropical gyre in the South Atlantic Ocean. *Journal of Marine Research*, 43:57–65, 1985.

M. Uda and K. Hasunuma. The Eastward Subtropical Countercurrent in the Western North Pacific Ocean. *Journal of the Oceanographical Society of Japan*, 25(4):201–210, 1969.

V. K. Valsala and M. Ikeda. Pathways and Effects of the Indonesian Throughflow Water in the Indian Ocean Using Particle Trajectory and Tracers in an OGCM. *Journal of Climate*, 20(13):2994–3017, July 2007. ISSN 0894-8755. doi: 10.1175/JCLI4167.1.

E. van Sebille, J. Sprintall, F. U. Schwarzkopf, A. S. Gupta, A. Santoso, M. H. England, A. Biastoch, and C. W. Böning. Pacific-to-Indian Ocean connectivity: Tasman leakage, Indonesian Throughflow, and the role of ENSO. *Journal of Geophysical Research: Oceans*, pages 1365–1382, 2014. doi: 10.1002/2013JC009525.Received.

A. M. Waite, P. A. Thompson, S. Pesant, M. Feng, L. E. Beckley, C. M. Domingues, D. Gaughan, C. E. Hanson, C. M. Holl, T. Koslow, M. Meuleners, J. P. Montoya, T. Moore, B. A. Muhling, H. Paterson, S. Rennie, J. Strzelecki, and L. Twomey. The Leeuwin Current and its eddies: An introductory overview. *Deep Sea Research Part II: Topical Studies in Oceanography*, 54(8-10):789–796, Apr. 2007. ISSN 09670645. doi: 10.1016/j.dsr2.2006.12.008.

A. J. Weaver and J. H. Middleton. On the Dynamics of the Leeuwin Current. *Journal of Physical Oceanography*, 19:626–648, 1989.

E. Weller, D. Holliday, M. Feng, L. Beckley, and P. Thompson. A continental shelf scale examination of the Leeuwin Current off Western Australia during the austral autumn–winter. *Continental Shelf Research*, 31(17):1858–1868, Nov. 2011. ISSN 02784343. doi: 10.1016/j.csr.2011.08.008.

M. Woo and C. Pattiaratchi. Hydrography and water masses off the western Australian coast. *Deep Sea Research Part I: Oceanographic Research Papers*, 55(9):1090–1104, Sept. 2008. ISSN 09670637. doi: 10.1016/j.dsr.2008.05.005.

M. Woo, C. Pattiaratchi, and W. Schroeder. Summer surface circulation along the Gascoyne continental shelf, Western Australia. *Continental Shelf Research*, 26(1):132–152, Jan. 2006. ISSN 02784343. doi: 10.1016/j.csr.2005.07.007.